



## Structure and mechanical behavior of human hair



Yang Yu<sup>a</sup>, Wen Yang<sup>b,c,\*</sup>, Bin Wang<sup>b</sup>, Marc André Meyers<sup>a,b,\*\*</sup>

<sup>a</sup> Department of NanoEngineering, University of California, San Diego, La Jolla, CA 92093, United States

<sup>b</sup> Materials Science and Engineering Program, University of California, San Diego, La Jolla, CA 92093, United States

<sup>c</sup> Department of Materials, Eidgenössische Technische Hochschule Zürich, Zürich 8093, Switzerland

### ARTICLE INFO

#### Article history:

Received 26 October 2016

Received in revised form 28 November 2016

Accepted 4 December 2016

Available online 9 December 2016

#### Keywords:

Keratin

Human hair

Mechanical properties

Strain-rate sensitivity

### ABSTRACT

The understanding of the mechanical behavior of hair under various conditions broadens our knowledge in biological materials science and contributes to the cosmetic industry. The hierarchical organization of hair is studied from the intermediate filament to the structural levels. The effects of strain rate, relative humidity, and temperature are evaluated. Hair exhibits a high tensile strength, 150–270 MPa, which is significantly dependent on strain rate and humidity. The strain-rate sensitivity, approximately 0.06–0.1, is comparable to that of other keratinous materials and common synthetic polymers. The structures of the internal cortex and surface cuticle are affected by the large tensile extension. One distinguishing feature, the unwinding of the  $\alpha$ -helix and the possible transformation to  $\beta$ -sheet structure of keratin under tension, which affects the ductility of hair, is analytically evaluated and incorporated into a constitutive equation. A good agreement with the experimental results is obtained. This model elucidates the tensile response of the  $\alpha$ -keratin fibers. The contributions of elastic and plastic strains on reloading are evaluated and correlated to structural changes.

© 2016 Elsevier B.V. All rights reserved.

### 1. Introduction

Hair, an important part of our body, not only possesses aesthetic significance in our culture, but also offers protection. This fiber-reinforced nanocomposite plays a key role as an outer covering in many vertebrates [1]. Hair fibers have a typical hierarchical structure similar to other  $\alpha$ -keratin materials, such as wool, nails, claws, and horns present in mammals. The keratin in reptiles and birds is primarily in the form of  $\beta$ -sheets [2]. Keratinous materials are categorized as  $\alpha$ -keratin if they exhibit a helical secondary structure or as  $\beta$ -keratin if they are in the shape of sheets. A typical hair fiber has a diameter of 50–100  $\mu\text{m}$  and is covered by an outermost layer, the cuticle. The cuticle consists of thin overlapping scales [3]. Each scale has an average length of 60  $\mu\text{m}$  and a thickness of about 0.5  $\mu\text{m}$ . Furthermore, 5–10 such scales overlap to create a total thickness of  $\sim 5 \mu\text{m}$ . The morphology of the cuticle edges is thought to be affected by weathering, combing, and brushing, with more severe damage seen on long hair fibers [4].

Fig. 1 shows the hierarchical structure of hair. The inner section of hair is called cortex and is composed of cortical cells that are  $\sim 100 \mu\text{m}$

long and 1–6  $\mu\text{m}$  thick. These cortical cells are composed of subcomponents called macrofibrils. The macrofibrils exhibit a diameter of 0.1–0.4  $\mu\text{m}$  [5]. At the nanometer scale, they are composed of intermediate filaments (IF) embedded in a matrix with high-sulfide content. One IF has a diameter of  $\sim 7.5 \text{ nm}$  and is formed by eight protofilaments. Each protofilament is composed on its turn of four right-handed  $\alpha$ -helix chains; therefore a total of thirty-two chains form an IF [6].

Hair fibers have 65–95 wt% of proteins depending on the humidity and up to 32% of water, with the rest as lipid pigments and other components [7]. Therefore, chemically the properties of human hair are dominated by the  $\alpha$ -keratin [8]. It has been demonstrated that the tensile properties of hair are mostly produced by the cortex, not the cuticle. Robbins and Crawford [9] damaged the cuticle with chemicals and found no apparent difference in the tensile properties with original hair fibers. Relaxation tests by Barnes and Roberts [10] and Robinson and Rigby [11] showed that the moduli are dependent on the time as well as strain and that the thiol content affects the mechanical properties. It was also demonstrated that the tensile properties are highly dependent on the influences of various factors: a high relative humidity decreases the Young's modulus and increases the extensibility [12]; an increase in temperature leads to a decrease in Young's modulus and an increase in extensibility [13]; twisting creates damage to the hair fibers [14] and this effect leads to the decrease in the breaking stress, breaking strain and Young's modulus. Ethnicities and age also affect the properties of human hair. It has been shown that hair specimens from different ethnicities exhibit different strains at cuticle lift off [15],

\* Correspondence to: W. Yang, Department of Materials, Eidgenössische Technische Hochschule Zürich, Zürich 8093, Switzerland.

\*\* Correspondence to: M.A. Meyers, Department of NanoEngineering, University of California, San Diego, La Jolla, CA 92093, United States.

E-mail addresses: [wen.yang@mat.ethz.ch](mailto:wen.yang@mat.ethz.ch) (W. Yang), [mameyers@eng.ucsd.edu](mailto:mameyers@eng.ucsd.edu) (M.A. Meyers).

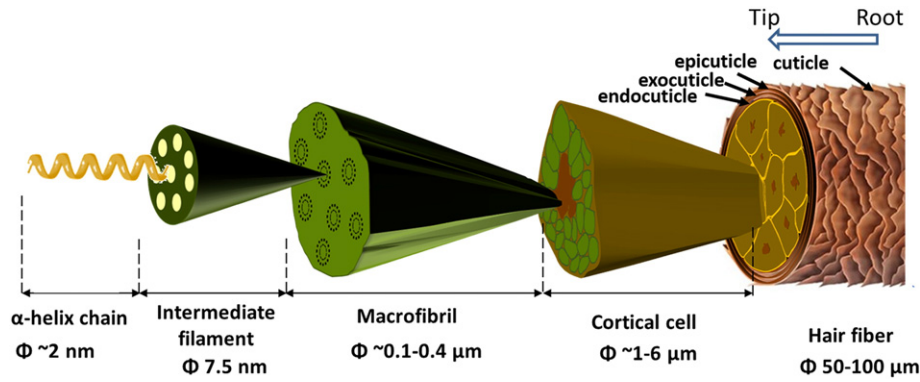


Fig. 1. Schematic representation of hierarchical structure in human hair starting at  $\alpha$ -helix chains and progressing to the entire section.

topographies [16–18], surface roughness [16], nanomechanical properties [19], and tensile properties [17,18]. In the meantime, as hair specimens age, the relaxation time also varies significantly [20].

Being one of the most important typical  $\alpha$ -keratin fibers, the mechanical behavior of hair was therefore studied quantitatively with respect to various contributing factors in this study. We report the sensitivities of the hair on the strain rate, relative humidity, and temperature through tensile testing. We also propose a constitutive equation for human hair and compare its predictions with experimental results.

## 2. Materials and methods

### 2.1. Specimen preparation

Hair specimens were collected from an East-Asian female in her early 30s. All the hair in the experiments was donated from only one individual to avoid the variations in mechanical properties reported between hairs from different ethnicities and the effect of aging as discussed above. No additional treatment such as straightening or dyeing except daily cleaning was conducted on the hair before collection. The average length of the collected hair was about 30 cm. Before specimen preparation, 2 cm sections were cut off at both ends from the entire hair and discarded. The remainder of the fiber was sectioned into 3 cm long pieces. For each small section, the two ends were glued into sand paper to prevent slipping between the grips during the tensile testing, leaving a 1.0–1.5 cm long hair span between sand papers to be tested. The cross-section area of each fiber was individually gauged using a 0–25 mm range micrometer with 0.001 mm accuracy. At least three measurements were made on one sample to ensure an average value in the diameter. It should also be noted that the pressing on the fiber was carefully avoided during measurements.

Specimens were tested under 20%, 50% (ambient) relative humidity (RH), and immersion in water at different strain rates. Specimens tested under water were first prepared by using the same method described above; additionally, the sand papers at the two ends were mounted into epoxy to prevent splitting in water. The hair fibers were then immersed in deionized (DI) water for 24 h to reach a full saturation before the mechanical tests. A transparent environmental chamber with a dehydrator and hydrometer was built to produce the low-humidity condition. The hair specimens were pre-treated at 20% RH for 3 days to ensure equilibrium with the environment and tested under such condition.

### 2.2. Mechanical testing

An Instron 3342 system with a 500 N load cell was used for tensile testing. Specimens were tested at strain rates of  $10^{-4}$ ,  $10^{-3}$ ,  $10^{-2}$ ,  $10^{-1}$ ,  $10^0$   $s^{-1}$  at room temperature and humidity. To determine the effect of humidity on the mechanical properties of hair, the pre-soaked specimens were tested in the DI water at 20 °C at varying strain rates.

The effect of temperature on the hair was established at a strain rate of  $10^{-2}$   $s^{-1}$  in order to maintain a steady temperature of the hair specimen during one tensile test. Tests at higher temperatures (40°, 60° and 80 °C) were conducted in water immersion. Cyclic mechanical tests in air at different temperatures were also conducted by using hair specimens which were heated with a common hair dryer while the temperature was monitored with a thermometer. At least five to eight specimens were tested under one condition (for example, each strain rate at each relative humidity) to ensure an accurate representation of the mechanical properties.

### 2.3. Characterization

For structural characterization, hair specimens were fractured in liquid nitrogen and then fixed using an established method [21]. The specimens were first immersed in 2.5% glutaraldehyde solution for 3 h and further dehydrated with an ascending ethanol series (30, 50, 70, 90, 95 and 100 vol.% twice) for 20 min in each solution. The surface (cuticle) of the hair before and after testing as well as the fracture surface of the hair specimens was observed in a FEI SFEG ultrahigh-resolution scanning electron microscopy (SEM) (FEI, Hillsboro, OR, USA). The specimens were sputtered with iridium prior to observation.

The hair was also characterized by transmission electron microscopy (TEM) using osmium tetroxide ( $OsO_4$ ) staining [22] with post-staining of lead. Segments of hair fibers were pre-treated by immersing in 0.5 M thioglycolic acid (pH 5.5) for 24 h at room temperature to enhance the contrast between the filaments and matrix. They were then washed with double-distilled water for 1 h and immersed in 1–2% aqueous  $OsO_4$  for 3 days. Afterwards, the segments were washed with distilled water, dehydrated to 100% ethanol through a series of graded alcohol solutions and then transitioned to 100% acetone through graded mixtures of ethanol and acetone. The specimens were subsequently infiltrated using Spurr's low viscosity epoxy resin through a series of solutions with increasing amounts of resin and decreasing amounts of acetone (25% resin + 75% acetone, 50% resin + 50% acetone, 75% resin + 25% acetone, 90% resin + 10% acetone, 100% resin, 100% resin), each taking one day. Specimens were then placed in fresh resin and polymerized for 2 days at 65 °C. The embedded specimens were trimmed and sectioned on a Leica Ultracut UCT ultramicrotome using a diamond blade. Sliced sections were picked up and post-stained with lead for 60 s. A FEI Technai 12 (Spirit) (120 kV) transmission electron microscope was used for examination.

## 3. Results and discussion

### 3.1. Structural and morphological characterization

Fig. 2 shows transmission electron micrographs of transverse cross section of hair. Within cortical cells, which are separated by a cell

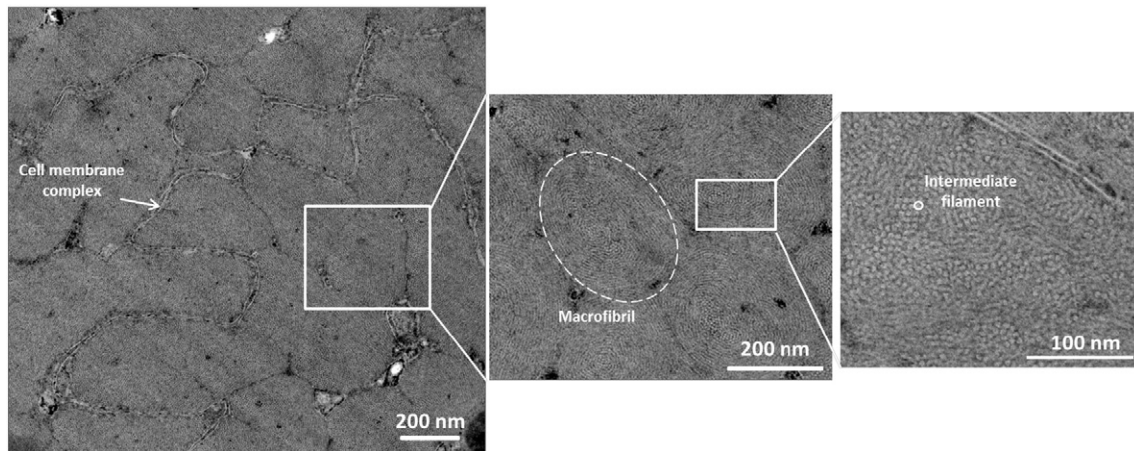


**Fig. 2.** Transmission electron micrographs (TEM) of human hair showing the cell membrane complex and intermediate filaments (high magnifications on the right).

membrane complex (the boundaries are marked in micrograph), there are approximately 20,000 intermediate filaments. Two lines are shown between cells, each corresponding to a cell wall (indicated by arrows in Fig. 2). The darker regions correspond to the remains of organelles and possibly cell nuclei. There is also an intermediate structure, macrofibrils, with a diameter of  $\sim 250$  nm, formed by the IFs. At the highest magnification, the circles with  $\sim 7$  nm diameter correspond to the intermediate filaments. They are connected by non-crystalline molecules and there seems to be a profusion of S-bonds that provide strong bonding between them [23,24].

Fig. 3a and b shows the structure of cuticle on a transverse surface after the hair was fractured in liquid nitrogen; macrofibrils of a hair fiber can be identified after the cross section was exposed (Fig. 3c and d). The original hair with a diameter of  $\sim 90$   $\mu\text{m}$  has a layered cuticle structure; sheets overlap and form a lamellar structure surrounding the central cortex (Fig. 3a). A higher magnification SEM micrograph (Fig. 3b) shows that the scales of this sample are broken and the edges are damaged. Fig. 3c shows a fractured surface of the hair. Cortical

cells with several micrometers in diameter align parallel to the direction of hair growth. A higher resolution image in Fig. 3d shows the macrofibrils in the cortical cells. These macrofibrils exhibit a diameter close to  $\sim 0.5$   $\mu\text{m}$  (indicated by arrows) and are tightly attached to each other even after the cortical cells are torn apart. The structural characterization reveals that the hair has a compact architecture in hierarchy with the scales on the surface.

### 3.2. Mechanical properties under different conditions

#### 3.2.1. Effect of strain rate

For a thorough understanding of the viscoplasticity of human hair, specimens were tested at different strain rates and temperatures. Typical stress-strain curves are summarized by the band plots in Fig. 4a and b, which incorporate the variation among specimens and indicate the effect of strain rate. As reported previously and also confirmed by our results, a typical tensile stress-strain curve of one hair fiber shows three regions. First it shows a linear section (up to  $\sim 0.02$ – $0.05$  strain),

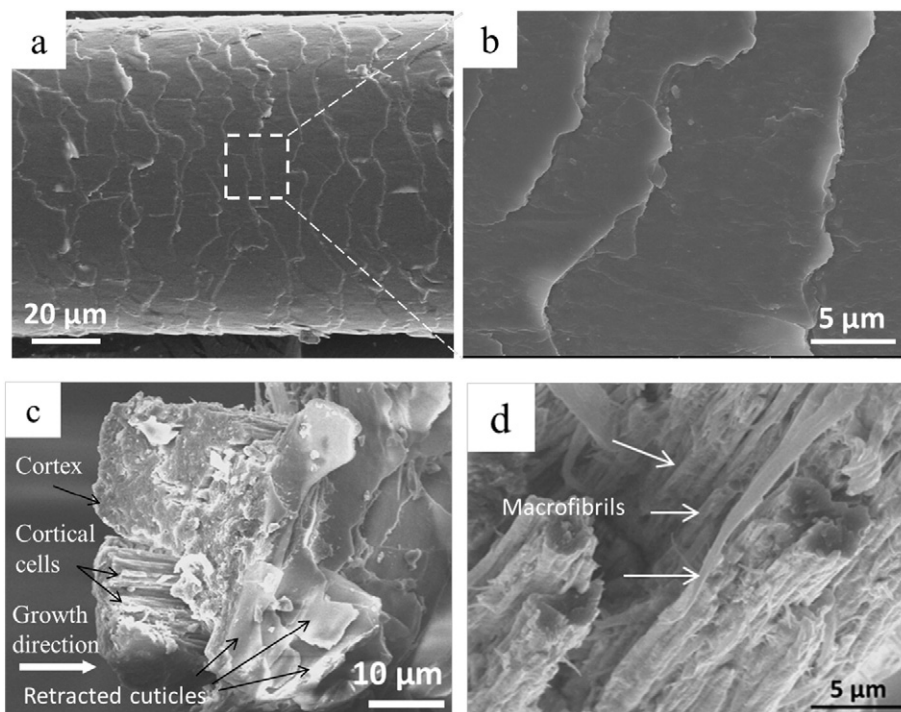


**Fig. 3.** SEM images of (a) and (b) cuticles at different magnifications, (c) cross section, and (d) macrofibrils (indicated by arrows) of a human hair fiber.

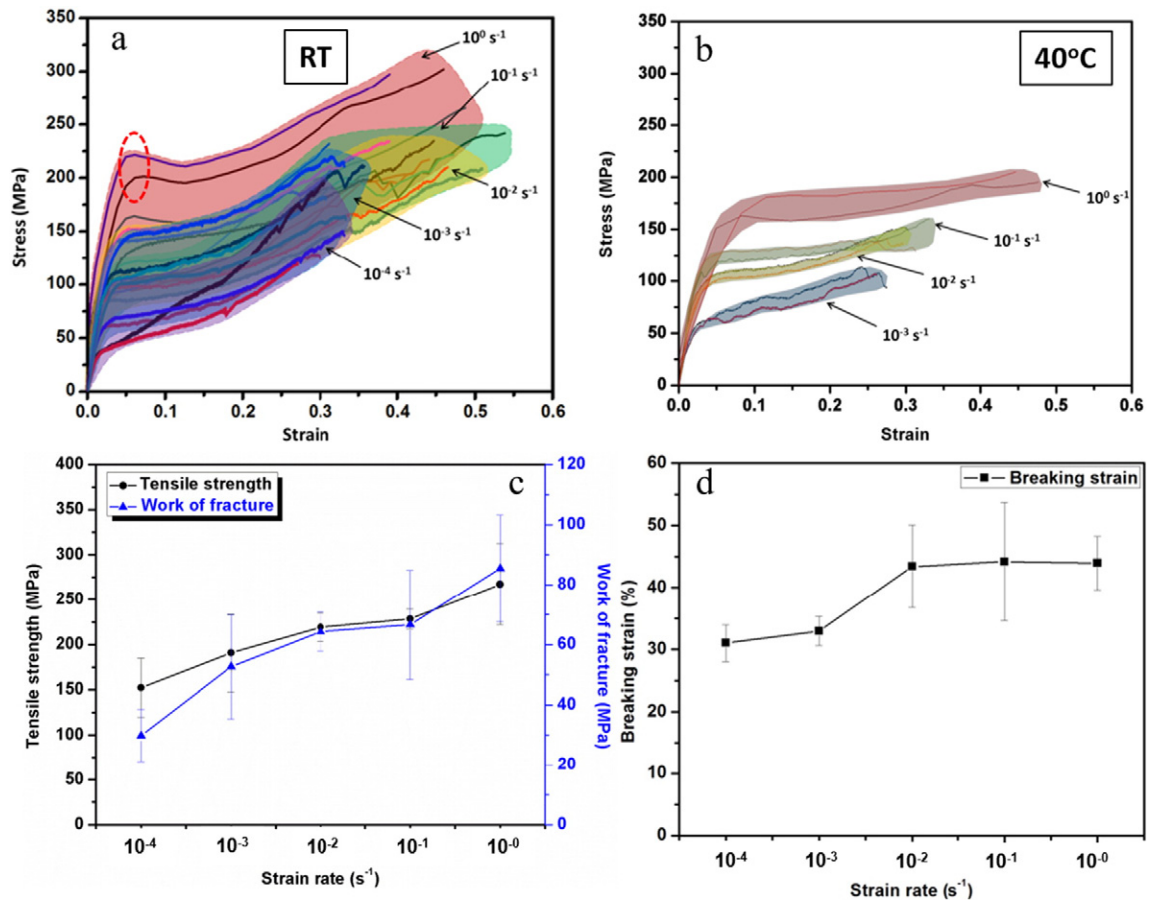


**Fig. 4.** Band plots of tensile results of human hair at (a) room temperature and (b) 40 °C, and (c) tensile strength, work-of-fracture and (d) breaking strain as a function of strain rate at room temperature (error bars represent standard deviation).

in which hair behaves mostly elastically. The chemical bonds are rearranged and no significant structural change is observed. The curve then goes into a transformation region where the  $\alpha$ -helix coils uncoil and may transform into  $\beta$ -sheets if conditions are conducive [8,25]. This region shows a very slow increase in stress with strain. After a certain strain ( $\sim 0.25$ ), the curve starts to show an increase in slope and enters the post-transformation region where mostly the remaining  $\alpha$ -helices and/or the  $\beta$ -sheets are stretched until the hair reaches the ultimate breaking point. As the strain rate increases, the stress of the “plateau” of the transformation region increases significantly. It is of note that at the highest strain rate ( $10^0 \text{ s}^{-1}$ ) there is a peak (circled in Fig. 4a) at  $\sim 0.05$  strain followed by a decrease in stress. This behavior becomes more apparent in curves with higher yield stress (the stress at 0.02 strain offset). This peak in stress may correspond to the critical stress of the intermediate filaments proposed in the Chapman/Hearle (C/H) model [26]. According to the C/H model, a critical stress needs to be reached in order to initiate the transformation from  $\alpha$ -helix to  $\beta$ -sheet and this is a characteristic of first-order phase changes. Chapman and Hearle [26,27] also indicated that a critical force is needed to initiate the formation of  $\beta$ -crystal nucleation. Beyond this critical point, the  $\alpha$ -helices will be uncoiled and this may lead to the formation of  $\beta$ -sheets region. This explains the decrease in stress after those peaks since the force drops back to the equilibrium value if transformation occurs. On the other hand, this behavior is only obvious in the tensile tests at  $10^0 \text{ s}^{-1}$  with a yield stress higher than  $\sim 150$  MPa, suggesting that there could be a critical stress for the sudden nucleation of the  $\beta$ -crystals. For curves with lower yield stress, the transformation region only shows a gradual increase in stress after the elastic region, which may indicate the uncoiling of the  $\alpha$ -helices and/or a gradual transformation to the  $\beta$ -sheets. Especially, tensile tests at lower strain rates

( $10^{-4}$  and  $10^{-3} \text{ s}^{-1}$ ) do not show a sharp turnover point between the transformation and post-transformation regions, which is thought due to a possibly continuous  $\alpha$ - $\beta$  transformation before the fracture. At a higher temperature of 40 °C (Fig. 4b), the hair shows a deteriorated performance in both yield stress and ultimate stress at each strain rate compared to that at room temperature. Despite the difference in temperature, there is a similar trend in the strain-rate sensitivity.

Fig. 4c shows the tensile strength and work-of-fracture (area under the stress-strain curve) as a function of strain rate at room temperature. For the lowest strain rate ( $10^{-4} \text{ s}^{-1}$ ), hair exhibits a tensile strength of  $152 \pm 33$  MPa and a work-of-fracture of  $30 \pm 9$  MPa. As the strain rate increases, the tensile strength shows an increase to  $267 \pm 45$  MPa (at  $10^0 \text{ s}^{-1}$ ). These results clearly confirm the viscoplasticity of hair: tensile strength increases with increasing strain rate. It corresponds to the relaxation tests conducted by Barnes and Roberts [10], proving that the tensile response of hair is strain-rate sensitive. Work-of-fracture shows a similar trend as the tensile strength. Fig. 4d shows that as the strain rate increases from  $10^{-4} \text{ s}^{-1}$  to  $10^0 \text{ s}^{-1}$ , the breaking strain first increases from 0.31 to 0.43 and then remains constant at  $\sim 0.45$ . This indicates that although the extensibility of hair is strain-rate sensitive, it can only increase to a certain value ( $\sim 0.45$ ) under the ambient condition.

### 3.2.2. Effect of humidity

The effect of relative humidity (RH) on the tensile properties was examined by testing hair specimens at 20% RH and in water at room temperature (20 °C). After the hair is soaked in water, it exhibits a swelling effect as the diameter increases by  $\sim 10\%$ . Fig. 5a shows three typical stress-strain curves at 20% RH, ambient humidity (50% RH) and water. At 20% RH, the hair exhibits a much higher yield stress and tensile stress compared to 50% and saturated condition. When the hair was tested in

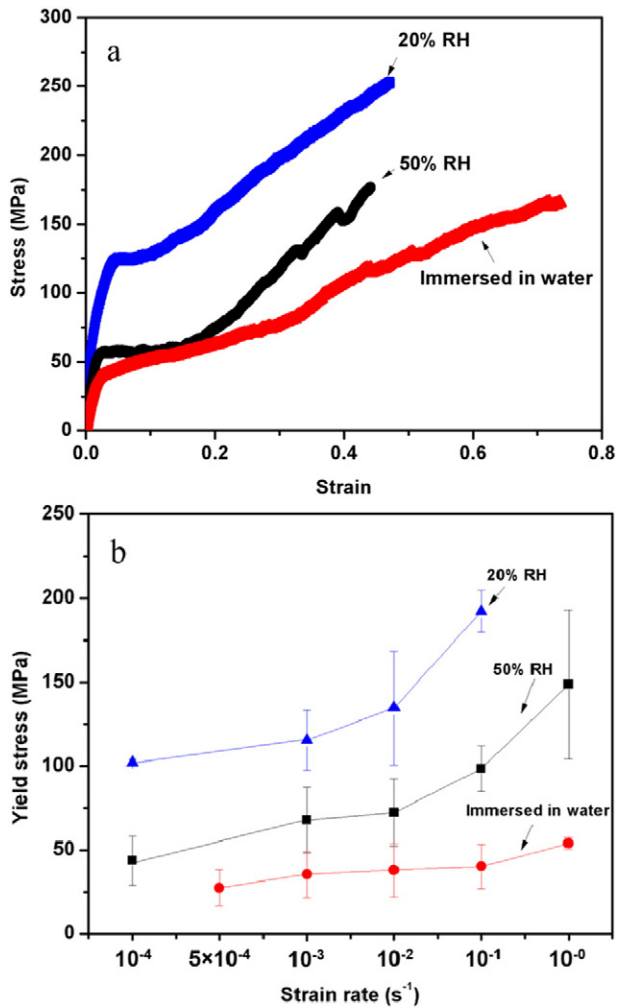


Fig. 5. (a) Typical stress-strain curves at different relative humidities and (b) yield stress as a function of strain rate (error bars represent standard deviation).

water, the Young's modulus was decreased and the hair fractured at a much lower stress. On the other hand, the hair exhibited a more extended post-plateau region and broke at a much larger strain ( $\sim 0.75$ ) compared to the ambient humidity ( $\sim 0.45$ ). Previous studies [28,29] suggest that the IFs are crystalline and not water sensitive, but the matrix proteins are thought to be affected more by water. According to Feughelman and Robinson [30,31], water works as plasticizer and reduces the interaction between protein chains; at the same time it also works as a swelling agent to increase the dimensions of keratin network. Therefore, water reduces the stiffness and increases the mobility of molecular structure of matrix by increasing the spacing between IFs and by plasticizing the amorphous matrix [31–33].

### 3.2.3. Strain-rate sensitivity

Hair specimens were further tested at three humidity levels under different strain rates ( $10^{-4}$  to  $10^0$  s<sup>-1</sup>) and the results are shown in Fig. 5b. For each strain rate, the yield stress decreases with increasing relative humidity. At the saturated condition, the yield stress increases from 28 MPa at  $5 \times 10^{-4}$  s<sup>-1</sup> to 54 MPa at  $10^0$  s<sup>-1</sup>; the increase of stress is much lower compared to 50% RH (44 MPa at  $10^{-4}$  s<sup>-1</sup> and 149 MPa at  $10^0$  s<sup>-1</sup>) and 20% RH (102 MPa at  $10^{-4}$  s<sup>-1</sup> and 192 MPa at  $10^{-1}$  s<sup>-1</sup>), which indicates that human hair has different strain-rate sensitivities at different humidities. The corresponding strain-rate sensitivities ( $m = \frac{\partial \log(\sigma)}{\partial \log(\dot{\epsilon})}$ ) of hair are 0.06, 0.11 and 0.08 at saturation and relative humidities of 50% and 20%, respectively.

The strain-rate sensitivities under various conditions are summarized in Fig. 6. Since hair is a bio-polymer, we compare its strain-rate sensitivity to that of two common polymers reported by Mulliken and Boyce [34]. The replotted data shown in Fig. 6 indicate that the strain-rate sensitivity of human hair as a natural polymer is comparable to other synthetic polymers. The pangolin scale, also keratinous [35], shows a strain-rate sensitivity of 0.08, which is in the same range as hair.

### 3.2.4. Effect of temperature in water

To understand the influence of temperature on human hair, specimens were tested at 20, 40, 60 and 80 °C at the same strain rate of  $10^{-2}$  s<sup>-1</sup>. This strain rate allows a uniform heat distribution in the hair and ensures a steady temperature in the water environment. Fig. 7 shows the stress-strain curves at various temperatures under water immersion. As the curve shifts downwards with increasing temperature, the yield stress and breaking stress decrease significantly. At 40 °C, the yield stress decreases from 39 MPa at 20 °C to 19 MPa; however, the yield stress only shows a slight decrease (15.5 MPa at 60 °C and 15.4 MPa at 80 °C), as the temperature further increases to 60 °C and beyond. This phenomenon is due to a glass transition reported at 35 °C [36, 37] and a further structural transition in  $\alpha$ -keratin around 60 °C [38–40]. This explains the decrease in yield stress from 20 to 40 °C as the water works as plasticizer and affects the amorphous matrix in the hair. It was found for wool that, as the temperature is increased to 60 °C, the ductility decreases [38], opposite to the character of glass transition. It was confirmed by X-ray examination that this is due to a structural change in the crystalline intermediate filaments. A simulation of the  $\alpha$ -helical structure in vacuum also confirmed that a high temperature of 67 °C destabilized and changed the helical conformation significantly [40]. This transition is thought to cause the decrease of yield stress between 40 and 60 °C. Akkermans and Warren [41] also confirmed that the yield stress of hair decreased with increasing temperatures using a two-state model simulation.

To further study the reversibility of such transition, another group of specimens were first immersed in water at 80 °C for at least 5 min, cooled down in 20 °C water and tested. The inserted diagram in Fig. 7b shows the comparison between three groups: hair tested at (a) 20 °C, (b) 80 °C and (c) heated-cooled (80–20 °C) hair. The third group showed no difference in yield stress compared to the second group (both  $\sim 16$  MPa). These last two groups have a much lower yield stress than hair tested at 20 °C (38 MPa). This result indicates that after heating to a high temperature, the human hair undergoes an irreversible structural change, which inevitably lowers the tensile strength and creates permanent damage.

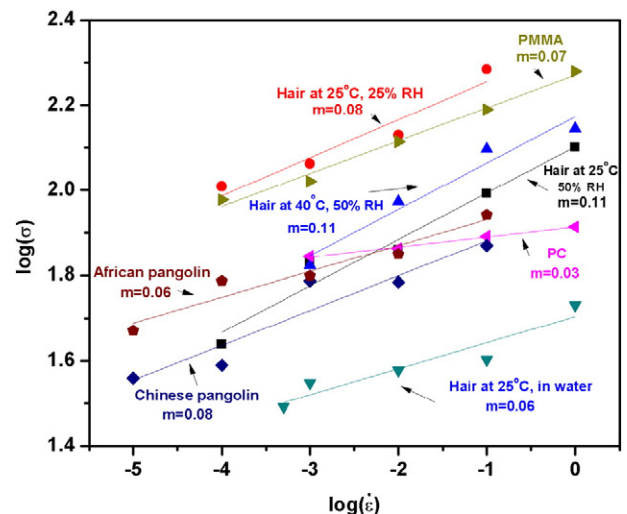


Fig. 6. Strain-rate sensitivities of human hair tested under various conditions, PMMA, PC, PMMA (adapted from [34]) and pangolin scales [35].

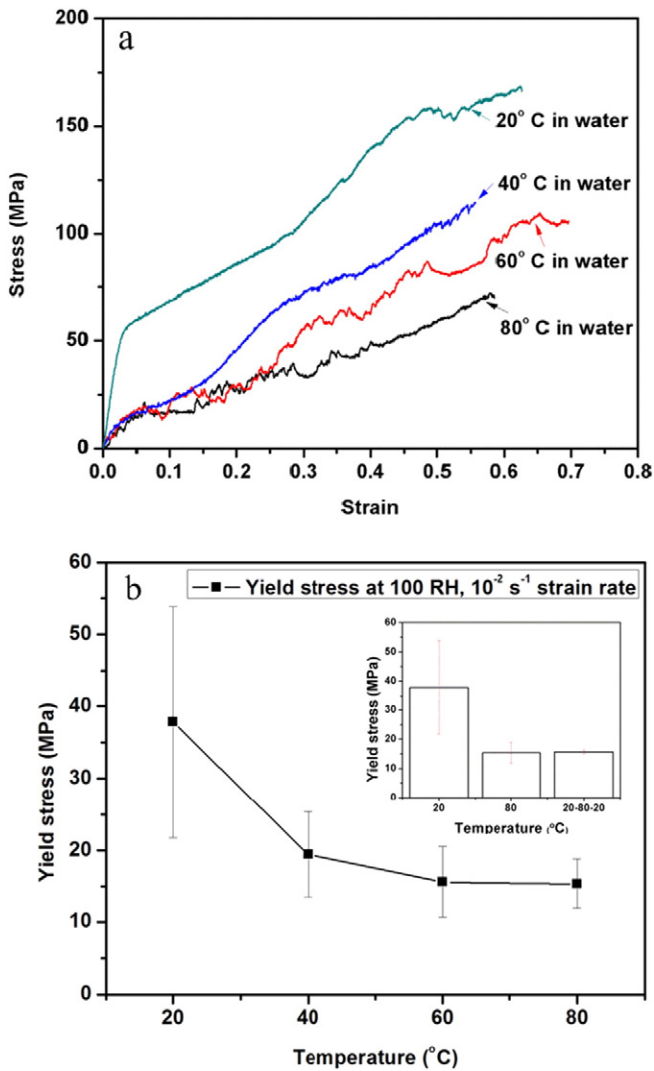


Fig. 7. (a) Representative stress–strain curves of hair under different temperatures in water and (b) yield stress as a function of temperature (inserted figure shows the comparison between room temperature, heated and heated-cooled conditions) (error bars represent standard deviation).

### 3.2.5. Load cyclic effect at different temperatures

In order to investigate the reversibility of the  $\alpha$ - $\beta$  transformation, specimens were stretched to strains of 0.01 and 0.1 at room temperature, unloaded, and reloaded at strain rate of  $10^{-3} \text{ s}^{-1}$ . These two strains represent the complete elastic and the plateau (transformation) regions, respectively. Fig. 8a shows the three cycles of loading–unloading at a strain of 0.01. These stress–strain curves all exhibit a linear behavior, with the same Young's modulus of  $\sim 4.2 \text{ GPa}$ . At this experimental condition, after each cycle, the specimens return to their original length and only the bonds of  $\alpha$ -helix are stretched within this region. The process is highly reversible and does not create plastic transformation in the structure.

The loading–unloading stress–strain curves up to 0.1 strain are shown in Fig. 8b. In the first cycle, the hair exhibits a similar Young's modulus of  $4.1 \text{ GPa}$  and a linear elastic region up to  $\sim 0.025$  strain, followed by the transformation region with a slow increase in stress up to 0.1 strain. Upon unloading, the curve shows a residual strain of  $\sim 0.06$ , indicating the partial reversibility of the deformed structure. In the subsequent two cycles, there is also a hysteresis in the unloading–reloading curve. The linearity of the unloading curve is lost due to the partially reversible changes, which results in a difference from the loading curve. Moreover, there is a significant decrease in yield stress as the

specimens are reloaded. Thus, the mechanical strength degrades in this partial phase reversal through the generation of flaws. The recovered strain in each cycle is  $\sim 0.03$ , which is close to the strain of elastic region. These results confirm that the  $\alpha$ - $\beta$  transformation is only partially reversible upon unloading.

Loading–unloading tests were also conducted at 40 and 60 °C and the results are shown in Fig. 8c and d, respectively; higher temperature does not contribute to a better reversibility in the  $\alpha$ - $\beta$  transformation. Moreover, at 60 °C, the mechanical strength of hair deteriorates significantly compared to that at lower temperatures, as the hair fractured during the 3rd cycle. The hysteresis in unloading–reloading produced by  $\beta$  to  $\alpha$  transformation is marked by arrows in Fig. 8. It is assumed that the decrease of yield stress upon reloading comes from damage in previous cycles or during unloading.

### 3.2.6. Weibull analysis among individuals of the same ethnicity

Although it has been noticed that there are variations in the hair properties among different ethnicities [15–19], the variation among the same ethnicity has not been well studied. Fig. 9 shows the Weibull fits of the yield stress of three females (#1 as the specimen donor above mentioned, #2 as an Eastern Asian female in her late 20s and #3 as an Eastern Asian female in her early 30s). These people were chosen due to their approximately same age group. The same number of specimens (8) from each individual were tested and plotted in the graph. The Weibull moduli, which indicate the variability of the same group of specimens, are 4.50, 4.50, and 5.92 for #1, #2, and #3 individuals, respectively. This shows that the variabilities of the three groups of specimens are within the same range. At the 50% probability of failure, the three individuals exhibit yield stresses of 94.8 MPa, 97.5 MPa, 90.5 MPa, respectively. Hence, the mechanical properties of hair from different individuals of the same ethnicity exhibit a very small difference statistically, and the current study is applicable to a broad spectrum of subjects.

### 3.3. Fracture surface and cuticle morphology

The fracture mechanisms at different strain rates were studied by examining the fracture surfaces. Fig. 10(a–e) shows the fracture surfaces of the specimens from low strain rate ( $10^{-4} \text{ s}^{-1}$ ) to high strain rate ( $10^0 \text{ s}^{-1}$ ) and Fig. 10f shows the schematic drawings of three modes of fracture identified. According to Kamath and Hornby [42], there are five fracture modes of human hair: split-ends, fibrillated, angle (Fig. 10a and b), step (Fig. 10c and d) and smooth (Fig. 10e). At low strain rates ( $10^{-4}$  and  $10^{-3} \text{ s}^{-1}$ ), hair behaves as a ductile material and shows an angle-end fracture mode (Fig. 10a and b). As the strain rate increases, the hair starts to show a step-end mode (Fig. 10c and d). The cortical cells break at different time during elongation to produce such fracture mode. However, at the high strain rate of  $10^0 \text{ s}^{-1}$ , the fracture surface exhibits a flat end (Fig. 10e), indicating a sharp split. This mode resembles the fracture surface of a brittle material. This indicates that the inter-fiber sliding, which takes place at low strain rates, is inhibited at high strain rates. The matrix material, being amorphous, shows significant strain-rate sensitivity, whereas the fibers can be considered as strain-rate insensitive. These results suggest that the fracture of cortical cells spreads gradually between neighboring cells until the whole hair is broken. The changes in the fracture surfaces ranging from low strain rate to high strain rate are illustrated in Fig. 10f. This embrittlement of the keratin at higher strain rates has been observed earlier by Seki et al. [43] for toucan beak keratin and Wang et al. [35] for pangolin scale.

The surface morphology change of hair cuticle at various strains was monitored using an *ex-situ* method. At a small strain (0.02), the cuticles do not show any lifting in the edges (Fig. 11a). However, as the strain increases to 0.15 (Fig. 11b) and 0.35 (Fig. 11c), the edges start to lift off and the surface becomes rougher; such a change is shown in the schematic drawing in Fig. 11d. This was also confirmed by an *in-situ* AFM

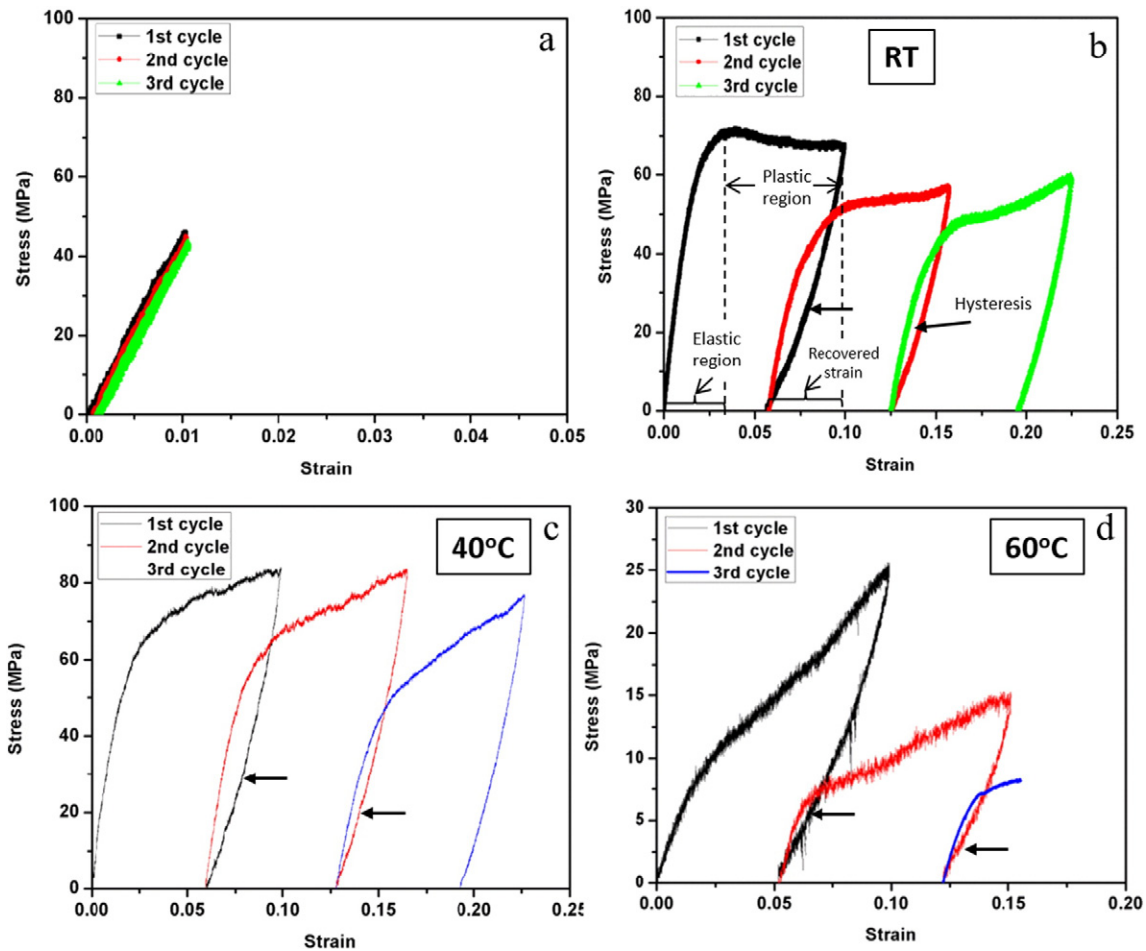


Fig. 8. Cyclic tensile tests up to (a) 0.01 and (b) 0.1 at 20 °C and cyclic tests up to 0.1 strain at (c) 40 °C and (d) 60 °C (hysteresis marked by arrows.).

study [15]. The phenomenon is thought to be due to different extensibilities in the layered cuticle structure. During elongation, the separation of these layers in the cuticle causes the roughness in the cuticle surfaces [15].

Furthermore, the effect of temperature on the cuticles was studied by observing the surface morphology near the fracture sites. At low temperatures (20 and 40 °C), the hair clearly shows the cuticle edges near the fracture sites (Fig. 12a and b). However, as the temperature

increases to 60 °C (Fig. 12c) and 80 °C (Fig. 12d), the edges of cuticle scales become undiscernible, which suggests that high temperature somehow has a ‘fusing’ effect on them. This further confirms that higher temperature not only changes the mechanical properties in hair, but also affects the surface morphology.

#### 4. Analysis

##### 4.1. Strain associated with $\alpha$ to $\beta$ transformation

The parameters of  $\alpha$ -helix and  $\beta$ -sheet keratin are shown in Fig. 13. The right-handed  $\alpha$ -helical molecule, which is prevalent in the elastic region, has a diameter of ~1.2 nm and periodicity of 0.52 nm in one turn (Fig. 13a). Once fully transformed, it turns into a  $\beta$ -sheet structure (Fig. 13b) and exhibits a periodicity of 0.7 nm with ~0.2 nm in thickness. During the transformation, 3.6 residues of one turn in  $\alpha$ -helix will experience an elongation in length from 0.52 nm (Fig. 13c) to 1.2 nm (Fig. 13d) in  $\beta$ -sheet structure. Therefore, the nominal strain of a theoretical full transformation from  $\alpha$ -helix to  $\beta$ -sheet structure is

$$\frac{1.2 \text{ nm} - 0.52 \text{ nm}}{0.52 \text{ nm}} = 1.31 \quad (1)$$

However, such high strain in the theoretically-complete transformation was not observed in the current experiments (Fig. 4a). We propose the following reasons for this phenomenon:

- The tensile stress may induce an unraveling in the  $\alpha$ -helices instead of transformation into  $\beta$ -sheets. Kreplak et al. [8] observed that at a high strain (above 20%) the  $\alpha$ -helical coils experience an unraveling

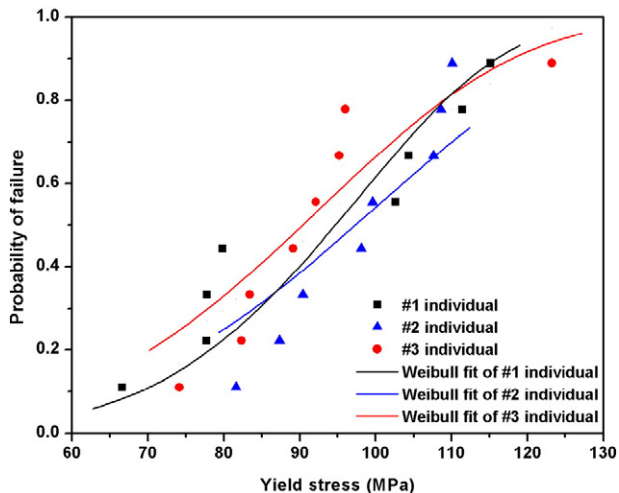
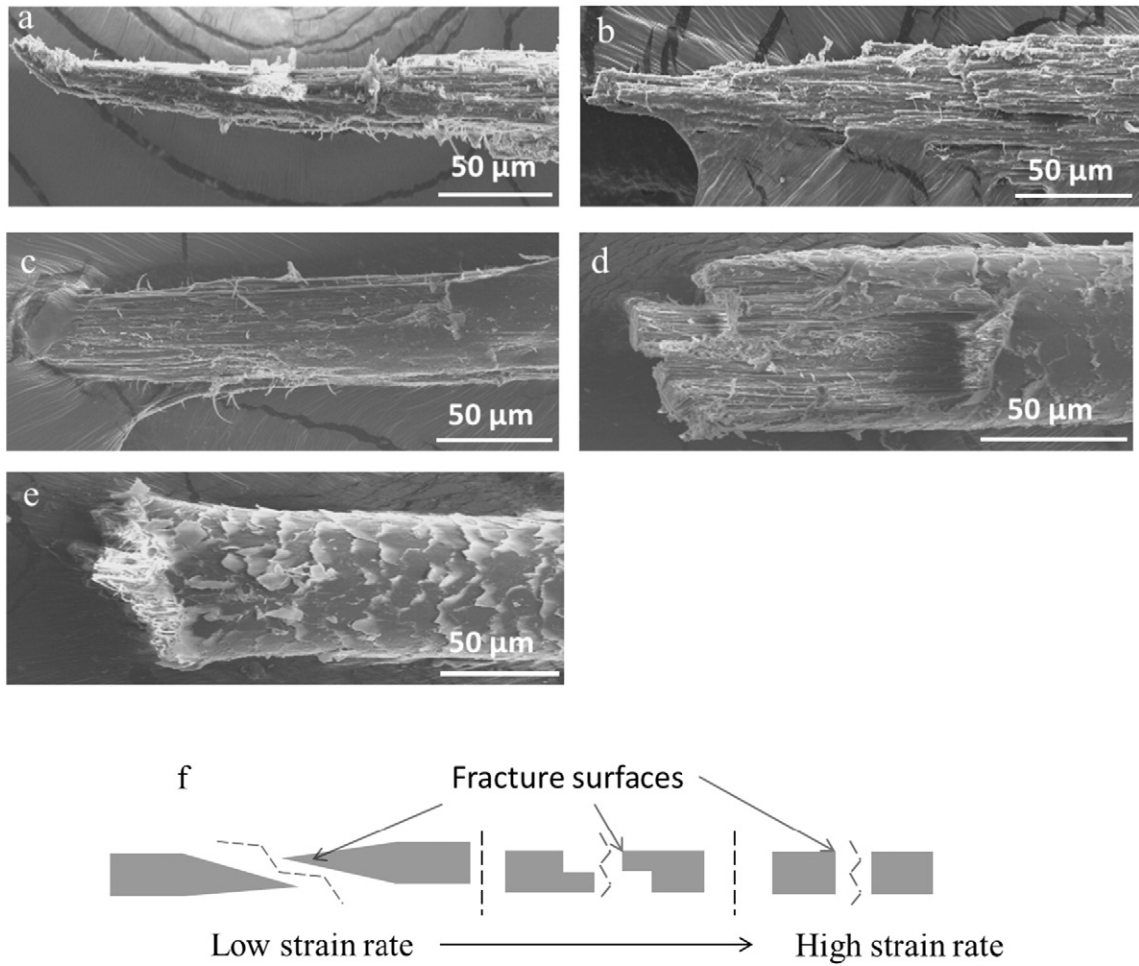
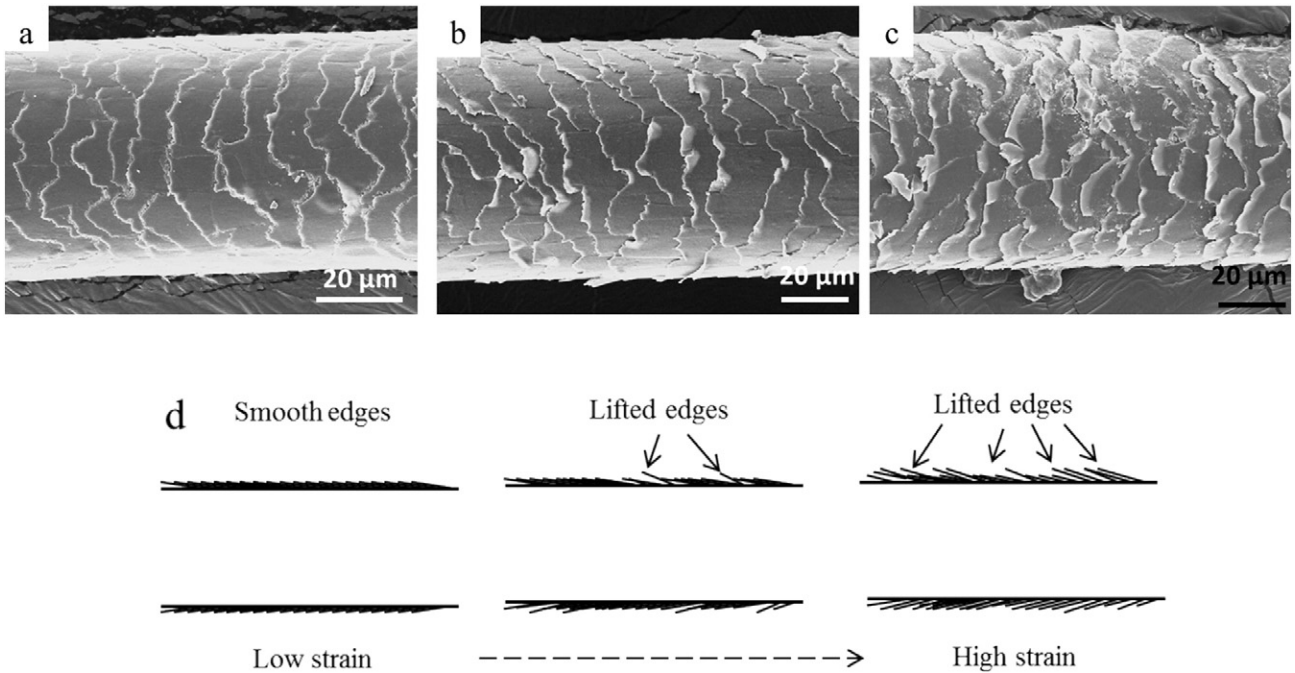


Fig. 9. Weibull analysis of three female individuals of the same ethnicity.



**Fig. 10.** Fracture surface of hair specimen tested at (a)  $10^{-4}$ , (b)  $10^{-3}$ , (c)  $10^{-2}$ , (d)  $10^{-1}$ , and (e)  $10^0 \text{ s}^{-1}$  strain rates and (f) schematic representations of fracture modes from low strain rate to high strain rate (at low strain rates, fiber pulling and inter-fiber sliding is more prominent. At high strain rates, fracture surface is flat).



**Fig. 11.** Surface morphology examined *ex-situ* under SEM at (a) 0.02, (b) 0.15, and (c) 0.35 strains and (d) illustration of scale edge lifting process.

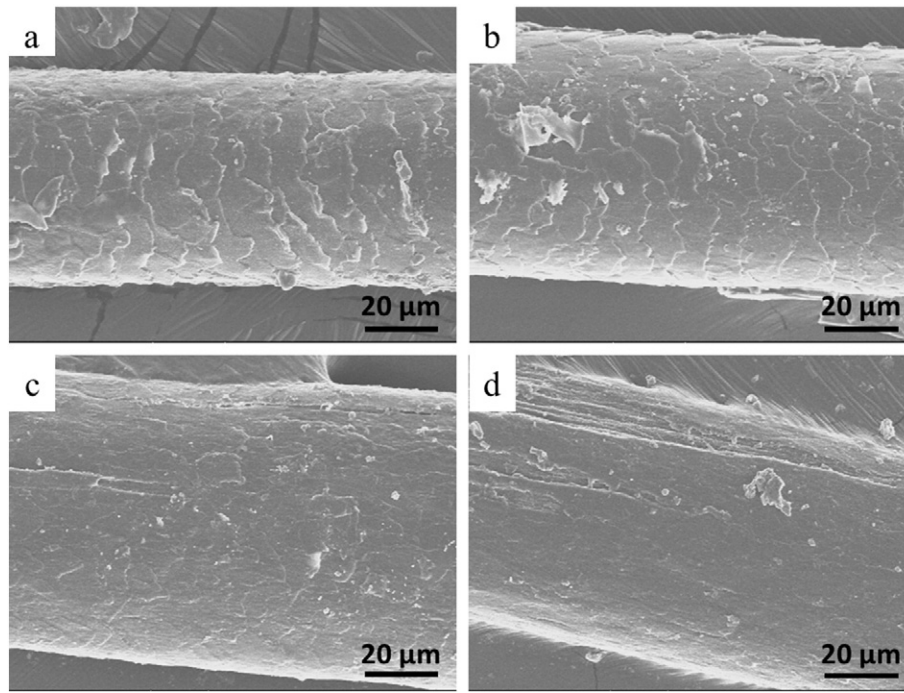


Fig. 12. Surface morphology near fracture sites, samples were tested at (a) 20 °C, (b) 40 °C, (c) 60 °C, and (d) 80 °C in water.

in the structure instead of a phase transition. It is also noted in their work that under conditions with low relative humidity the former could be the dominant effect in the keratinous fibers.

- ii. A complete transformation for all  $\alpha$ -helices to  $\beta$ -sheets may not be achievable. In the experiments, this transformation may be only local and not uniform along the entire specimen. During the post-transformation region, the newly-transformed  $\beta$ -sheets are extended and contribute to the tensile response even though the transformation is not complete.
- iii. The experimental condition may not be conducive to a full  $\alpha$ - $\beta$  transformation. Kreplak et al. [25] showed that under steam condition, horse hair was able to achieve 100% extension. Fig. 5a also shows that at a higher humidity, the human hair exhibits a larger extensibility. It is possible that the ambient condition in the current experiments is not suitable for the full  $\alpha$ - $\beta$  transformation, since the breaking strain is also highly dependent on temperature and strain rate, as shown previously.
- iv. The inherent structure, orientation and properties of intermediate filaments (IFs) are not conducive to a full  $\alpha$ - $\beta$  transformation. Hair is composed of numerous IFs which consist of periodic  $\alpha$ -helical and non-helical regions [2]; only the  $\alpha$ -helices have the potential to transform to  $\beta$ -sheets and thus contribute to the tensile strain. In addition, the IFs do not possess exactly the same orientation (Fig. 2) and mechanical properties; therefore the IFs that are well aligned with the hair axis will elongate while others may not. Moreover, some IFs would break earlier than others, which creates defects in the hair so that the hair breaks before the full  $\alpha$ - $\beta$  transformation is completed. The loading-unloading-reloading experiments suggest the existence of permanent damage during tensile tests.

Since the  $\alpha$ - $\beta$  transformation takes place during the transformation region, which ends at  $\sim 0.25$  strain, the transformation ratio,  $r$ , along the fiber direction by the end of this region can be obtained as the following:

$$r = \frac{0.25}{1.31} = 0.19 \quad (2)$$

This ratio expresses the fraction of  $\alpha$ -helices that are fully transformed into  $\beta$ -sheets during the tensile tests.

Wide-angle X-ray scattering (WAXS) patterns for hair before and after stretching are shown in Fig. 14 to help to understand the  $\alpha$ - $\beta$  transformation during the tensile tests. Prior to tensile testing,  $\alpha$ -keratin in human hair exhibits a spot at 0.96 nm indicating the distance between adjacent  $\alpha$ -helices and another meridian arc at 0.52 nm embedded into a broader one around 0.5 nm [25]. Fig. 14a shows the typical  $\alpha$ -keratin X-ray diffraction pattern in human hair before stretching. However, after stretching, the 0.52 nm meridian arc becomes less obvious and another equatorial arc at 0.465 nm appears, corresponding to the distance between  $\beta$ -sheets (Fig. 14b). This indicates that the keratin in hair experiences a transformation from  $\alpha$ -helices to  $\beta$ -sheets during stretching.

#### 4.2. Constitutive equation of the tensile response

A constitutive equation based on the experimental results of hair is proposed to obtain a better quantitative description of the tensile properties of similar  $\alpha$ -keratin fibers. Firstly, the hair is simplified into only two components: IFs and matrix, as illustrated in Fig. 15a by Feughelman [30,44]. The IFs and matrix are considered as parallel and aligned with each other and these components can be analyzed individually using the separate stress-strain curves proposed by Wortmann and Zahn [45]. As shown in Fig. 15b, the intermediate filaments are characterized by three stages: (a) a near linear region up to 0.02 (elastic region) which only involves the change of bond angles without significant structural transformation, (b) a flat region with little increase in stress (transformation region) due to the  $\alpha$ - $\beta$  transition, and (c) an increase in stress until the ultimate breaking stress (post-transformation region). On the other hand, the amorphous matrix shows a relatively high modulus at small strain and a gradual rise in stress as the strain further increases.

Based on the model developed by Feughelman, Wortmann and Zahn [30,45], we establish the following equation for a typical stress-strain curve. Therefore, at each strain  $\varepsilon$ :

$$\sigma = E_1\varepsilon + E_2(\varepsilon - \varepsilon_{c1})H(\varepsilon_{c1}) + E_3(\varepsilon - \varepsilon_{c2})H(\varepsilon_{c2}) \quad (3)$$

where  $\varepsilon_{c1}$  and  $\varepsilon_{c2}$  are the strains at elastic to transformation and transformation to post-transformation transitions ( $\varepsilon_{c1} = 0.02, \varepsilon_{c2} = \sim 0.25$  as

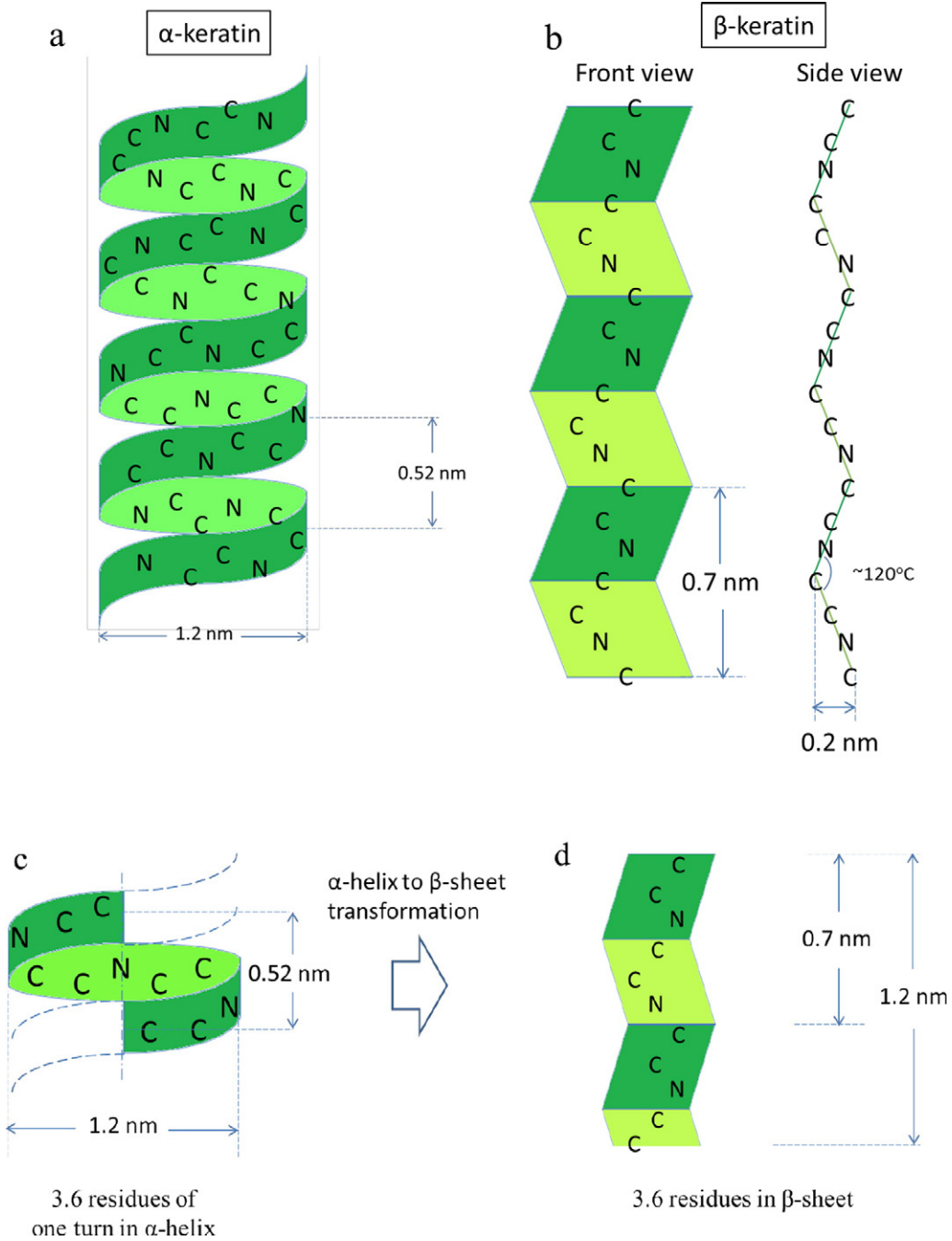


**Fig. 13.** Schematic representation of (a) α-helix and (b) β-sheet keratin in human hair and transformation of 3.6 residues from (c) α-helical to (d) β-sheet structure.

previously mentioned);  $H$  is a Heaviside function to activate the two terms [46] and  $E_1, E_2, E_3$  jointly define the moduli of the elastic, transformation and post-transformation regions. To obtain the yield stress and strain, we define the yield point as the intersection between the following two equations:

$$\begin{cases} \sigma = E_1 \varepsilon + E_2 (\varepsilon - 0.02) \\ \sigma = E_1 (\varepsilon - 0.02) \end{cases} \quad (4)$$

$$(5)$$

Therefore, we have

$$\sigma_y = \frac{-0.02 E_1^2}{E_2}, \varepsilon_y = \frac{0.02 E_2 - 0.02 E_1}{E_2}$$

As the slope is very small within the transformation region, we have  $E_1 + E_2 \approx 0; E_2 \approx -E_1$ , thus, the yield stress and strain can be further simplified to  $\sigma_y = 0.02 E_1$  and  $\varepsilon_y = 0.04$ .

Hair exhibits strain-rate sensitivity and thermal softening effects, as shown in Fig. 6; we introduce a strain-rate sensitivity and a thermal softening (adapted from Chen et al. [47]) functions as follows:

$$\sigma_y = \sigma_{iso} \left( \frac{\dot{\varepsilon}}{\dot{\varepsilon}_0} \right)^m \quad (6)$$

$$\sigma_y(T) = \sigma_{iso} \cdot C \cdot \exp \left[ \left( \frac{T - T_0}{T_m - T_0} \right)^\beta \right] \quad (7)$$

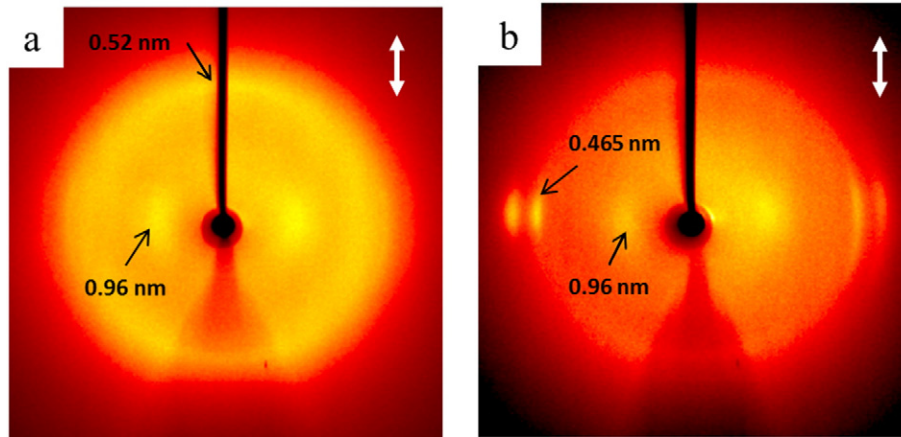


**Fig. 14.** Wide-angle X-ray scattering (WAXS) patterns of human hair (a) prior to and (b) after stretching to strain of 0.35 (fiber direction indicated by double-headed lines) (note that the reflection in meridian arc at 0.52 nm characteristic of  $\alpha$ -keratin and the one at 0.465 nm after deformation corresponding to  $\beta$ -keratin).

where  $\dot{\epsilon}_0 = 10^{-2} \text{ s}^{-1}$  is the reference strain rate;  $T_0 = 20 \text{ }^\circ\text{C}$  is the room temperature;  $T_m \approx 155 \text{ }^\circ\text{C}$  is the melting temperature at 100% RH [48].

Assuming that the strain rate and thermal softening contribute to the overall tensile properties individually, the constitutive equation is:

$$\sigma = \left\{ E_1(\dot{\epsilon}) \cdot \left( \frac{\dot{\epsilon}}{\dot{\epsilon}_0} \right)^m \cdot C \cdot \exp \left[ \left( \frac{T - T_0}{T_m - T_0} \right)^\beta \right] \right\} \varepsilon + E_2(\varepsilon - 0.02)H(0.02) + E_3(\varepsilon - 1.22r)H(1.22r) \quad (8)$$

The parameters of Eq. (8) are:  $\dot{\epsilon}_0 = 10^{-2} \text{ s}^{-1}$ ,

$$T_0 = 20 \text{ }^\circ\text{C},$$

$$T_m = 155 \text{ }^\circ\text{C},$$

$$E_1 = 4.7,$$

$$E_2 = -4.5,$$

$$E_3 = 0.25,$$

$$m = 0.06 \text{ (100% RH)},$$

$$C = 0.95,$$

$$\beta = -2.77,$$

$$r = 0.19.$$

Fig. 16 shows the prediction of Eq. (8), which incorporates the strain-rate, temperature, and transformation functions. The predicted stress-strain curves from this constitutive model agree reasonably with the experimental results at different strain rates.

Therefore, this equation effectively provides help in predicting and analyzing the tensile behavior of hair under various strain rates and temperatures.

## 5. Conclusions

In this present study, the tensile properties of human hair under various strain rates, relative humidities, and temperatures are investigated. A constitutive equation is developed based on these experimental results. The major contributions are summarized as follows:

- (i) The yield stress of hair decreases with decreasing strain rate, increasing relative humidity, and increasing temperature. The hair exhibits different strain-rate sensitivities at ambient humidity and in water indicating different responses of the amorphous matrix. Temperature affects the tensile properties at two critical values, a glass transition at  $35 \text{ }^\circ\text{C}$  and a further structural change

around  $60 \text{ }^\circ\text{C}$ . Moreover, results show that the structural change is not reversible even after the specimens are cooled back to  $20 \text{ }^\circ\text{C}$ .

- (ii) Cyclic mechanical tests show that the hair behaves both elastically and plastically within the elastic and transformation regions. These tests confirm that no substantial structural change is introduced during the elastic region since the deformation is completely reversible; as the  $\alpha$ -helical structure uncoils and transforms to  $\beta$ -sheets, it introduces a plastic deformation which is only partially recoverable upon unloading.
- (iii) A constitutive equation is developed based on the experimental results and the two-phase model proposed by Feughelman [30]. Strain-rate sensitivity and thermal softening are included and this model may advance our understanding in the analysis and prediction of the tensile behavior of similar  $\alpha$ -keratin fibers.

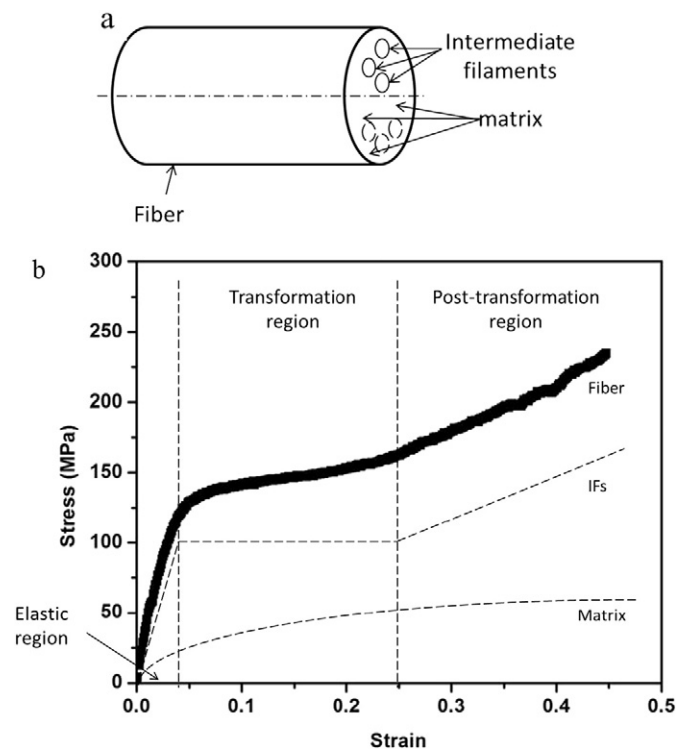


**Fig. 15.** (a) Two-phase composite model for a wool fiber (adapted from [30]) and (b) stress-strain curves proposed for IFs and matrix (adapted from [45]).

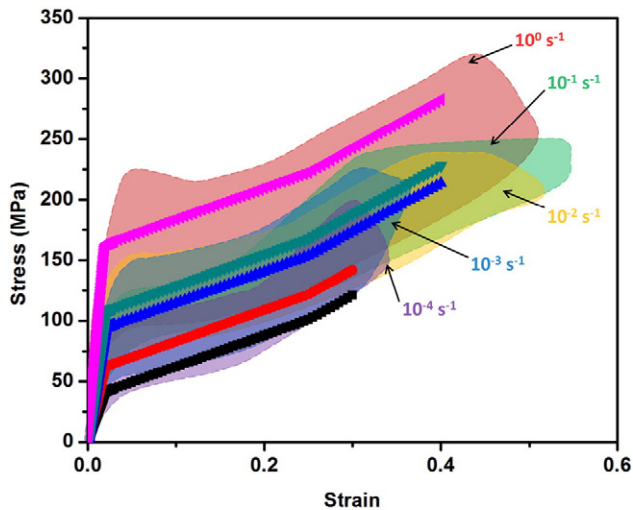


**Fig. 16.** Predicted (lines from top to bottom corresponding to  $10^0$ ,  $10^{-1}$ ,  $10^{-2}$ ,  $10^{-3}$ , and  $10^{-4}$   $s^{-1}$  strain rates, respectively) using two-phase constitutive equation and experimental (bands) showing tensile behaviors of human hair under different strain rates.

### Acknowledgement

We gratefully acknowledge the financial support from a Multi-University Research Initiative through the Air Force Office of Scientific Research (AFOSR-FA9550-15-1-0009) and support of Yang Yu by the Powell Foundation through Jacobs School of Engineering at UCSD. We thank Prof. Kenneth S. Vecchio for his input and discussions. We appreciate the help from Mason Mackey at the National Center for Microscopy and Imaging Research (NCMIR) for TEM specimen preparation and imaging. We thank Dr. Curtis Moore at UCSD Crystallography Facility for the assistance in the WAXS experiments.

### References

- [1] J. McKittrick, P.-Y. Chen, S.G. Bodde, W. Yang, E.E. Novitskaya, M.A. Meyers, The structure, functions, and mechanical properties of keratin, *JOM* 64 (2012) 449–468.
- [2] B. Wang, W. Yang, J. McKittrick, M.A. Meyers, Keratin: structure, mechanical properties, occurrence in biological organisms, and efforts at bioinspiration, *Prog. Mater. Sci.* 76 (2016) 229–318.
- [3] J.A. Swift, Human hair cuticle: biologically conspired to the owner's advantage, *J. Cosmet. Sci.* 50 (1999) 23–47.
- [4] M.L. Garcia, J.A. Epps, R.S. Yare, L.D. Hunter, Normal cuticle-wear patterns in human hair, *J. Soc. Cosmet. Chem.* 29 (1978) 155–175.
- [5] D.P. Harland, R.J. Walls, J.A. Vernon, J.M. Dyer, J.L. Woods, F. Bell, Three-dimensional architecture of microfibrils in the human scalp hair cortex, *J. Struct. Biol.* 185 (2014) 397–404.
- [6] D. Voet, J.G. Voet, *Biochemistry: Life at the Molecular Level*, third ed. John Wiley&Sons, New York, 2008.
- [7] M.V.R. Velasco, T.C. De Sá Dias, A.Z. De Freitas, N.D.V. Júnior, C.A.S. De Oliveira Pinto, T.M. Kaneko, A.R. Baby, Hair fiber characteristics and methods to evaluate hair physical and mechanical properties, *Braz. J. Pharm. Sci.* 45 (2009) 153–162.
- [8] L. Kreplak, J. Doucet, F. Briki, Unraveling double stranded  $\alpha$ -helical coiled coils: an X-ray diffraction study on hard  $\alpha$ -keratin fibers, *Biopolymers* 58 (2001) 526–533.
- [9] C.R. Robbins, R.J. Crawford, Cuticle damage and the tensile properties of human hair, *J. Soc. Cosmet. Chem.* 42 (1991) 59–67.
- [10] H.A. Barnes, G.P. Roberts, The non-linear viscoelastic behaviour of human hair at moderate extensions, *Int. J. Cosmet. Sci.* 22 (2000) 259–264.
- [11] M.S. Robinson, B.J. Rigby, Thiol differences along keratin fibers: stress/strain and stress-relaxation behavior as a function of temperature and extension, *Text. Res. J.* 55 (1985) 597–600.
- [12] C.R. Robbins, *Chemical and Physical Behavior of Human Hair*, Springer Science & Business Media, 2002.
- [13] L. Rebenfeld, H.D. Weigmann, C. Dansizer, Temperature dependence of the mechanical properties of human hair in relation to structure, *J. Soc. Cosmet. Chem.* 538 (1966) 525–538.
- [14] T.A. Dankovich, Y.K. Kamath, S. Ruetsch, Tensile properties of twisted hair fibers, *J. Cosmet. Sci.* 55 (2004) S79–S90 Suppl.
- [15] I.P. Seshadri, B. Bhushan, Effect of ethnicity and treatments on in situ tensile response and morphological changes of human hair characterized by atomic force microscopy, *Acta Mater.* 56 (2008) 3585–3597.
- [16] C. LaTorre, B. Bhushan, Nanotribological characterization of human hair and skin using atomic force microscopy, *Ultramicroscopy* 105 (2005) 155–175.
- [17] A. Franbourg, P. Hallegot, F. Baltenneck, C. Toutain, F. Leroy, Current research on ethnic hair, *J. Am. Acad. Dermatol.* 48 (2003).
- [18] L.J. Wolfram, Human hair: a unique physicochemical composite, *J. Am. Acad. Dermatol.* 48 (2003) 106–114.
- [19] G. Wei, B. Bhushan, Nanotribological and nanomechanical characterization of human hair using a nanoscratch technique, *Ultramicroscopy* 106 (2006) 742–754.
- [20] M. Benzarti, M.B. Tkaya, C.P. Mattei, H. Zahouani, Hair mechanical properties depending on age and origin, *World Acad. Sci. Eng. Technol.* (2011) 471–477.
- [21] W. Yang, V.R. Sherman, B. Gludovatz, E. Schaible, P. Stewart, R.O. Ritchie, M.A. Meyers, On the tear resistance of skin, *Nat. Commun.* 6 (2015) 1–10.
- [22] B.K. Filshie, G.E. Rogers, An electron microscope study of the structure of feather keratin, *J. Cell Biol.* 13 (1962) 1–12.
- [23] R.C. Marshall, D.F.G. Orwin, J.M. Gillespie, Structure and biochemistry of mammalian hard keratin, *Electron Microsc. Rev.* 4 (1991) 47–83.
- [24] J.W.S. Hearle, Protein fibers: structural mechanics and future opportunities, *J. Mater. Sci.* 42 (2007) 8010–8019.
- [25] L. Kreplak, J. Doucet, P. Dumas, F. Briki, New aspects of the  $\alpha$ -helix to  $\beta$ -sheet transition in stretched hard  $\alpha$ -keratin fibers, *Biophys. J.* 87 (2004) 640–647.
- [26] J.W.S. Hearle, A critical review of the structural mechanics of wool and hair fibres, *Int. J. Biol. Macromol.* 27 (2000) 123–138.
- [27] B.M. Chapman, A Mechanical Model, For wool and other keratin fibers, *Text. Res. J.* 39 (1969) 1102–1109.
- [28] R.S. Bear, H.J. Rugo, The results of x-ray diffraction studies on keratin fibers, *Ann. N. Y. Acad. Sci.* 53 (1951) 627–648.
- [29] P. Milczarek, M. Zielinski, M.L. Garcia, The mechanism and stability of thermal transitions in hair keratin, *Colloid Polym. Sci.* 270 (1992) 1106–1115.
- [30] M. Feughelman, A two-phase structure for keratin fibers, *Text. Res. J.* 29 (1959) 223–228.
- [31] M. Feughelman, M.S. Robinson, The relationship between some mechanical properties of single wool fibers and relative humidity, *Text. Res. J.* 37 (1967) 441–446.
- [32] M. Feughelman, *Mechanical Properties and Structure of Alpha-keratin Fibres: Wool, Human Hair and Related Fibres*, UNSW Press, Sydney, 1997.
- [33] J.E.A. Bertram, J.M. Gosline, Functional design of horse hoof keratin: the modulation of mechanical properties through hydration effects, *J. Exp. Biol.* 136 (1987) 121–136.
- [34] A.D. Mulliken, M.C. Boyce, Mechanics of the rate-dependent elastic-plastic deformation of glassy polymers from low to high strain rates, *Int. J. Solids Struct.* 43 (2006) 1331–1356.
- [35] B. Wang, W. Yang, V.R. Sherman, M.A. Meyers, Pangolin armor: overlapping, structure, and mechanical properties of the keratinous scales, *Acta Biomater.* 41 (2016) 60–74.
- [36] D.G. Phillips, Detecting a glass transition in wool by differential scanning calorimetry, *Text. Res. J.* 55 (1985) 171–174.
- [37] F.-J. Wortmann, M. Staples, R. Elliott, L. Chandra, The effect of water on the glass transition of human hair, *Biopolymers* 83 (2006) 371–375.
- [38] P. Mason, Thermal transitions in keratin part I: thermal expansion and structural transitions in alpha-keratin, *Text. Res. J.* 34 (1964) 913–917.
- [39] P. Mason, Thermal transitions in keratin: part II: thermal transitions in stressed keratin fibers, *Text. Res. J.* 34 (1964) 1021–1026.
- [40] B. Knopp, B. Jung, F.-J. Wortmann, Modeling of the transition temperature for the helical denaturation of  $\alpha$ -keratin intermediate filaments, *Macromol. Theory Simul.* 6 (1997) 1–12.
- [41] R.L.C. Akkermans, P.B. Warren, Multiscale modelling of human hair, *Phil. Trans. R. Soc. Lond. A.* (2004) 1783–1793.
- [42] Y.K. Kamath, S.B. Hornby, Mechanical and fractographic behavior of Negroid hair, *J. Soc. Cosmet. Chem.* 43 (1984) 21–43.
- [43] Y. Seki, S.G. Bodde, M.A. Meyers, Toucan and hornbill beaks: a comparative study, *Acta Biomater.* 6 (2010) 331–343.
- [44] M. Feughelman, Natural protein fibers, *J. Appl. Polym. Sci.* 83 (2002) 489–507.
- [45] F.-J. Wortmann, H. Zahn, The stress/strain curve of  $\alpha$ -keratin fibers and the structure of the intermediate filament, *Text. Res. J.* 64 (1994) 737–743.
- [46] M.A. Meyers, P.-Y. Chen, *Biological Materials Science*, Cambridge Press, 2014.
- [47] S. Chen, C. Huang, C. Wang, Z. Duan, Mechanical properties and constitutive relationships of 30CrMnSiA steel heated at high rate, *Mater. Sci. Eng. A* 483–484 (2008) 105–108.
- [48] J. Cao, F. Leroy, Depression of the melting temperature by moisture for  $\alpha$ -form crystallites in human hair keratin, *Biopolymers* 77 (2005) 38–43.